Title
Data assimilation of low-altitude magnetic perturbations into a global magnetosphere model

Journal
Space Weather, 14(2)

ISSN
1539-4956

Authors
Merkin, VG
Kondrashov, D
Ghil, M
et al.

Publication Date
2016-02-01

DOI
10.1002/2015sw001330

Peer reviewed

AGU PUBLICATIONS

Space Weather

RESEARCH ARTICLE
10.1002/2015SW001330

Key Points:
- Initial approach to data assimilation in a global magnetosphere model tested
- Low-altitude magnetic perturbations assimilated
- Approach found promising for assimilation of data sets like AMPERE

Correspondence to:
V. G. Merkin,
Slava.Merkin@jhuapl.edu

Citation:
Merkin, V. G., D. Kondrashov, M. Ghil, and B. J. Anderson (2016), Data assimilation of low-altitude magnetic perturbations into a global magnetosphere model, *Space Weather*, *14*, 165–184, doi:10.1002/2015SW001330.

Received 30 OCT 2015
Accepted 29 JAN 2016
Accepted article online 4 FEB 2016
Published online 29 FEB 2016

Data assimilation of low-altitude magnetic perturbations into a global magnetosphere model

V. G. Merkin[1], D. Kondrashov[2], M. Ghil[2], and B. J. Anderson[1]

[1]The Johns Hopkins University Applied Physics Laboratory, Laurel, Maryland, USA, [2]Department of Atmospheric and Oceanic Sciences and Institute of Geophysics and Planetary Physics, University of California, Los Angeles, California, USA

Abstract The ionosphere is the only region of the terrestrial magnetosphere-ionosphere system where in situ observations with high temporal resolution and approaching global spatial scale are possible. Ionospheric measurements of magnetic fields with such spatiotemporal coverage have become available from the Active Magnetosphere and Planetary Electrodynamics Response Experiment, combining data from the Iridium® satellites. Motivated by the emergence of this data set, we report here on the first results of assimilation of low-altitude ionospheric magnetic perturbations into the Lyon-Fedder-Mobarry (LFM) global magnetospheric model coupled with the Rice Convection Model (RCM). Our assimilation approach relies on the assumption of a quasi-steady, linear approximate relation between equatorial magnetospheric pressure and ionospheric Region 2 field-aligned currents. This approximation is implemented numerically by perturbing large-scale modes from the Fourier decomposition of equatorial magnetospheric pressures and computing responses of the corresponding modes in the ionospheric magnetic field. This methodology was validated by using model-based assimilation tests of the so-called "fraternal twins" type. In this approach, the LFM-RCM model with one set of parameters is used to generate synthetic observations, while a model version with different parameters is used to assimilate the ionospheric observations and calculate the magnetospheric pressure corrections which are then applied to reproduce the synthetic observations. The model with assimilated synthetic data responded correctly by modifying ionospheric currents and magnetic perturbations in the expected way. We thus found the approach proposed herein to be promising for future assimilation of real data.

1. Introduction and Motivation

The terrestrial magnetosphere is a strongly coupled nonlinear physical system populated by fully ionized plasmas immersed in the Earth's magnetic field. Together with the ionosphere, solar wind, and corona, they form the largest natural plasma laboratory accessible to in situ observations. Studies of this system are therefore of fundamental physical interest. The magnetosphere-ionosphere system is also home to geomagnetic disturbances that are primarily caused by this system's interaction with the solar wind. These disturbances are collectively called *space weather* whose extreme manifestations can have significant socioeconomic impacts.

Studying complex physical systems with a large number of degrees of freedom requires building computer models. The most complete description of the magnetosphere can in theory be achieved by solving the full set of Maxwell and Vlasov-Boltzmann equations using particle simulations throughout. Due to the extremely wide range of spatiotemporal scales involved—spanning 10^2–10^9 m and microseconds to days—this goal will remain elusive for the foreseeable future, at least for explicit codes [*Lapenta*, 2012].

The Vlasov description can be reduced to a single-fluid approximation by taking moments of the ion and electron distribution functions. This magnetohydrodynamic (MHD) approximation allows a global description of the magnetosphere, including its most basic structural elements such as the bow shock, the magnetopause, and the magnetotail. MHD-based computer models of the magnetosphere have been developed since the early days of space science [*LeBoeuf et al.*, 1978; *Lyon et al.*, 1981; *Ogino and Walker*, 1984] and have become the workhorses of magnetospheric and space weather research ever since [e.g., *Lyon et al.*, 2004; *Tóth et al.*, 2007; *Raeder et al.*, 2008; *Janhunen et al.*, 2012].

Global MHD magnetospheric models have matured to the point at which they can be used to predict space weather processes [e.g., *Pulkkinen and et al.*, 2011; *Rastätter et al.*, 2011]. These models, though, still face the problem of insufficiently or poorly specified boundary and initial data, as well as of incomplete physics.

To tackle this problem, the meteorological community has been developing methods of data assimilation (DA) for the past half century [e.g., *Bengtsson et al.*, 1981; *Ghil and Malanotte-Rizzoli*, 1991; *Daley*, 1996; *Kalnay*, 2006]. Methods of conventional data assimilation have also been applied successfully in space physics, particularly, in the ionosphere [e.g., *Richmond*, 1992; *Schunk et al.*, 2004; *Matsuo et al.*, 2015] and radiation belts [e.g., *Kondrashov et al.*, 2007; *Koller et al.*, 2007; *Godinez and Koller*, 2012; *Shprits et al.*, 2013]. The underlying idea of DA is to combine the model output with available measurements to construct an optimal estimate of the true state of the system. In global magnetospheric modeling, the development and implementation of DA methods have been hampered by the enormous range of spatial scales of the system and by the heretofore poor spatiotemporal coverage of available measurements.

The data scarcity problem is, however, partially mitigated by the mapping of the system electrodynamics along the magnetic field to the ionosphere. Because of its proximity to Earth, the ionosphere allows global continuous monitoring by spacecraft on a low Earth orbit and by ground-based facilities such as radars and magnetometers.

At the same time, the ionosphere is tightly coupled with the magnetosphere through magnetic field lines. The stresses generated in the solar wind and magnetospheric plasmas are transmitted to the ionosphere by means of Alfvén waves, which travel along these field lines and carry magnetic perturbations transverse to the zeroth-order geomagnetic field, as well as the corresponding field-aligned Birkeland currents. The electrically conducting ionospheric plasma allows horizontal closure of the Birkeland currents, which results in plasma convection. The corresponding convective electric field, in turn, maps to the magnetosphere and regulates plasma circulation there [e.g., *Wolf*, 1983]. These two factors—i.e., the availability of global continuous ionospheric observations and the tight physical coupling of ionospheric and magnetospheric processes—suggest the feasibility of assimilating ionospheric data into global magnetosphere models.

In this paper, we explore this possibility by concentrating specifically on assimilation of magnetic field perturbations at low, ionospheric altitudes. Our approach is motivated by the recent emergence of a new observational asset provided by the Active Magnetosphere and Planetary Electrodynamics Response Experiment (AMPERE). AMPERE uses high-cadence magnetometer data from the Iridium® constellation with its more than 70 satellites, and it yields low-altitude (~800 km) observations of magnetic perturbations with a global continuous coverage [*Anderson et al.*, 2000, 2014; *Waters et al.*, 2001]. Figure 1 illustrates conceptually the proposed DA approach.

There are a number of ways to assimilate this data set into a global model. First, the magnetic perturbations are necessary for the specification of the inner boundary conditions in global MHD models; this boundary is usually placed at an altitude of roughly 2 R_E. For instance, the Lyon-Fedder-Mobarry (LFM) model used herein sets this boundary condition by eliminating the derivative of the tangential component of the perturbation magnetic field along the boundary normal: $d\mathbf{B}_\tau/d\hat{\mathbf{n}} = 0$. Other types of boundary conditions have also been suggested recently [*Xi et al.*, 2015].

One can envisage assimilating the data at the boundary by nudging the simulation toward a better agreement with the data. The question is whether these corrections will propagate through the relevant volume of the magnetosphere. Although we have not investigated this question in detail, our preliminary results indicated that imposing boundary values for magnetic perturbations did not result in significant changes throughout the magnetosphere. We suspect that this lack of impact of the data is due to the fact that the generators of field-aligned currents (FACs) are located in the inner magnetosphere [e.g., *Roelof*, 1989] or at high latitudes at its boundary with the solar wind [e.g., *Lopez et al.*, 2011]. Apparently, the ionospheric boundary condition on the magnetic perturbations does not exercise a sufficiently strong feedback on the magnetospheric current generators to significantly alter the ionospheric FACs.

The alternative approach we took here is to "tweak" the magnetospheric current generators so as to optimally match the observed distribution of magnetic perturbations in the ionosphere. Based on the initial results described below, this approach appears promising and worthy of further investigation. Hence, we present herein an initial, proof-of-concept exploration of this approach to magnetospheric DA.

In this paper, we focus on the methodology and do not use the real AMPERE data but rather construct synthetic observations from a model that differs in some parameter values from the one that is used to assimilate the data. This allows us, on the one hand, to develop and test the DA approach independently of approaches to treat noise characteristics of the data; on the other hand, it maintains a degree of realism due to the

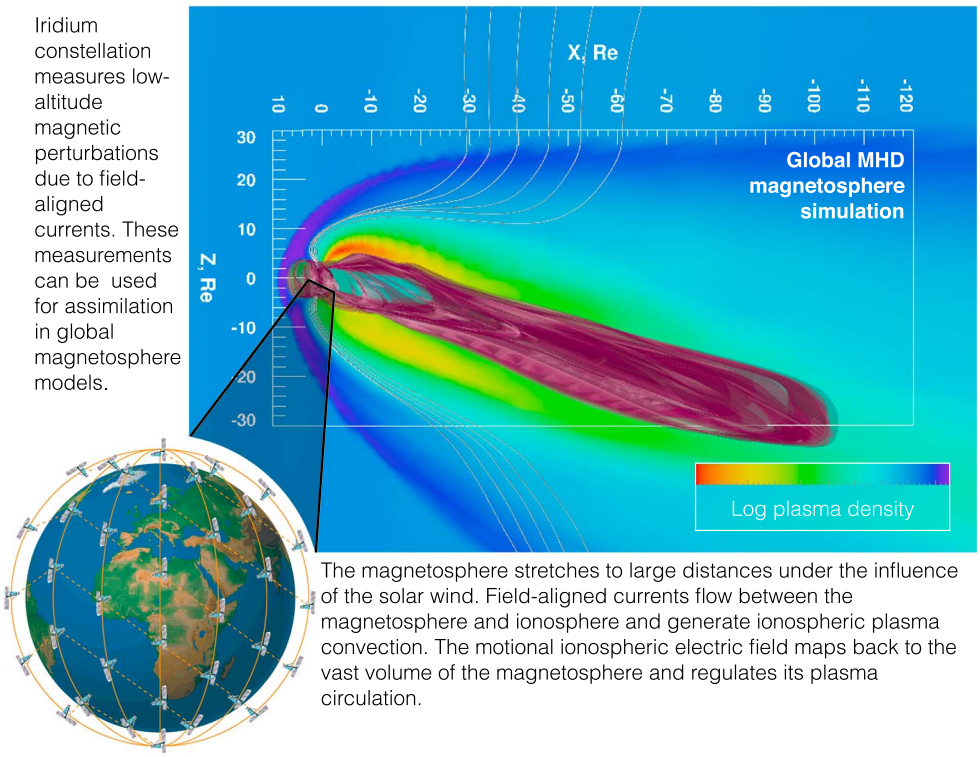

Figure 1. The Iridium spacecraft constellation provides global continuous measurements of magnetic perturbations at the low-altitude boundary of global MHD magnetosphere models. In this paper, we explore the possibility of assimilation of these data into a coupled magnetosphere-ionosphere model. Iridium constellation image credit: Iridium Communications Inc.

difference between the two model versions one of which plays the role of "truth" or "nature," the other the role of the actual model. Given the nature of the data set—namely, its global coverage and ~10 min time cadence [*Merkin et al.*, 2013; *Anderson et al.*, 2014]—we expect the application to real data provided by AMPERE to include a straightforward analysis of the error covariance which may, however, be labor intensive because it will require data spanning a broad range of geomagnetic conditions. Nonetheless, the global and approximately uniform distribution of the observations in the AMPERE data set implies that little if any effort will be needed to condition the assimilation to be stable in regions without data coverage.

The paper is organized as follows. Section 2 introduces our main methodological DA ideas. Section 3 reviews the models to be used, while section 4 describes the details of our DA method's implementation. Section 5 presents the results, and section 6 summarizes and concludes the work.

2. Assimilation Method Outline

Once the decision is made to adjust the current generators to the data, one has to address two questions: which generators and how to tweak them? Particularly during southward interplanetary magnetic field (IMF) conditions, the ionospheric currents are commonly described as consisting of a poleward situated Region 1 (R1) system and a Region 2 (R2) system equatorward of that [e.g., *Iijima and Potemra*, 1976, 1978]. While detailed classification of the R1 and R2 generation regions is not straightforward and depends on the magnetic local time (MLT) [*Ohtani et al.*, 2010; *Wing et al.*, 2010], generally, the R1 currents on the dayside are thought to be driven by the solar wind dynamo while R2 currents on the nightside and much of the dayside are driven by plasma pressure distributions within the magnetosphere. R1 polarity currents on the nightside are likely driven by some combination of magnetotail flows and pressure distributions. Figure 2 illustrates characteristic features of these two regions by using (a) the actually measured magnetic perturbations, (b) the spherical cap harmonic fit to these measurements, and (c) the corresponding FACs derived from the fit in Figure 2b.

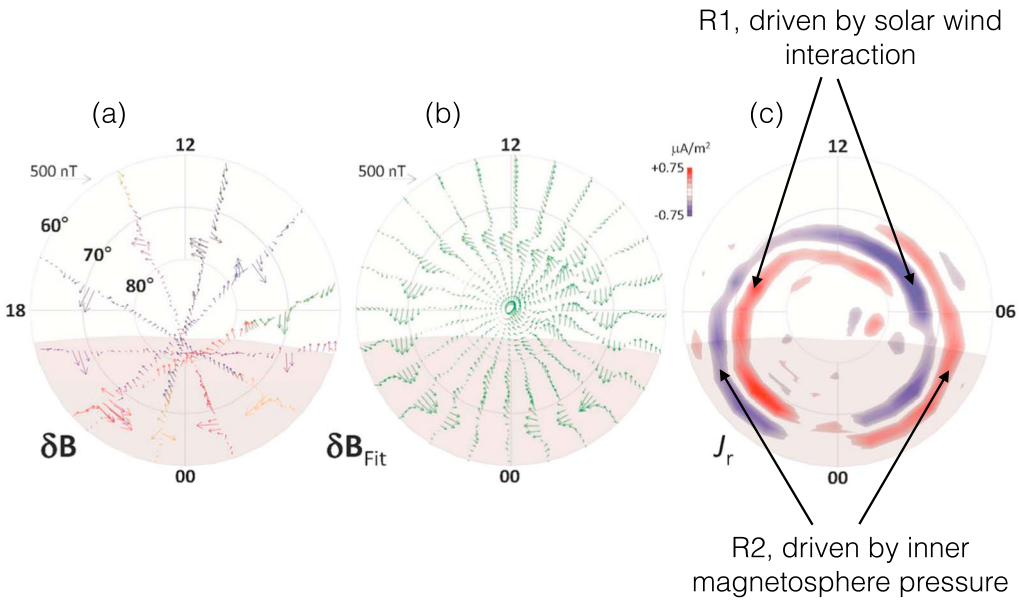

Figure 2. The typical two regions, R1 and R2, of the field-aligned current (FAC) system, based on data from the AMPERE experiment for 1920–1930 UT on 15 October 2015, adapted from *Anderson et al.* [2014]. (a) The actual magnetic perturbation ($\delta\mathbf{B}$) measured by the Iridium satellites, (b) spherical cap harmonic fit to these data, and (c) derived FACs [see *Anderson et al.*, 2014, for details]. Figure 2c shows the typical R1 + R2 current system and indicates that at least the dayside R1 currents are driven primarily by direct interaction with the solar wind, while the R2 currents are driven by inner magnetosphere pressure gradients.

In this initial study, we consider assimilation of ionospheric perturbations associated with the R2 current system whose primary driver is the plasma pressure in the inner magnetosphere [*Wolf*, 1983; *Roelof*, 1989; *Liemohn et al.*, 2001; *Toffoletto et al.*, 2003; *Sitnov et al.*, 2010]. This avoids the challenge of assimilating signals generated in the R1 system since that would also entail varying the solar wind and IMF parameters. Such a modification can probably be accomplished by an ensemble Kalman filter [*Evensen*, 2003], but it is not the approach explored herein. Eventually, assimilation approaches will need to be developed for both the R1 and R2 systems; here we concentrate on the latter specifically.

We assume that the outer boundary condition of the global MHD simulation is a fixed function $\mathbf{Q}(t)$ of time, and we do not subject it to variations $\delta\mathbf{Q}$ of the solar wind or the IMF parameters to match the ionospheric observations. Here $\mathbf{Q}(t)$ is the vector of all MHD quantities necessary to specify the outer boundary condition of the model. In other words, we assume that the R1 currents are a given feature of the simulation and make no attempt to modify their generation mechanisms.

We note that the above considerations do not presume that R2 currents are independent of external driving, since the pressure distribution generating R2 currents is ultimately produced by external driving. Rather, the assumption underlying our approach is that—for given solar wind and IMF conditions—the pressure distribution in the inner magnetosphere is imperfect in the model, and we use the information about the relevant ionospheric perturbations to correct it.

The inner magnetosphere is typically governed by the slow-flow approximation [*Wolf*, 1983]; hence, we can use quasi-static equations to describe both the system's evolution and our DA methodology for it. This approximation simplifies the problem by eliminating the feedback time scales that are faster than the AMPERE data time cadence of ~10 min; it also has the additional benefit of eliminating the magnetic field-aligned coordinate from the problem thus making it effectively two dimensional (2-D).

Subject to this approximation, and also assuming the plasma isotropy which is implied by our models, the FACs in the ionosphere are related to the magnetospheric pressure distribution by the Vasyliunas equation [*Vasyliunas*, 1970]:

$$\frac{j_{\parallel}}{B_{\mathrm{i}}} = c\frac{\hat{\mathbf{b}}}{2B_{\mathrm{m}}} \cdot \nabla V \times \nabla p, \tag{1}$$

where $j_{\parallel}$ is the ionospheric FAC, B_i and B_m are the magnitudes of the magnetic field at the ionosphere and in the magnetosphere, V is the flux tube volume, p is the scalar plasma pressure, and c is the speed of light. The FAC vector is, in turn, related to the measured magnetic perturbations as follows [*Waters et al.*, 2001]:

$$\mathbf{j}_{\parallel} = \frac{4\pi}{c} \nabla \times \delta \mathbf{B}. \tag{2}$$

Equations (1) and (2) collectively describe the steady state relationship between the magnetospheric pressure distribution and magnetic perturbations measured at low altitudes in the ionosphere, e.g., 780 km in case of Iridium satellites. These equations effectively constitute the reduced physical model into which we assimilate the data on the time scales of roughly 10 min, at which the quasi-steady approximation is valid.

A deep analogy exists, in fact, between the quasi-static MHD approximation, equation (1), and quasi-geostrophic balance relations in the atmosphere and oceans [*Ghil and Malanotte-Rizzoli*, 1991]: the underlying physical cause of this analogy is the neglect of the inertial terms in the dynamical equations of both planetary flows and MHD, along with the similar roles played in balancing pressure gradients by the Coriolis force from Earth's rotation [*Ghil and Childress*, 2009, and references therein] and the electromagnetic Lorentz force, respectively.

The Vasyliunas equation (1) is a steady state, isotropic, 2-D approximation to the full three-dimensional (3-D), time-dependent MHD model, which depends on the magnetic field distribution. Therefore, for our DA approach we rely numerically on a reduced representation of equation (1) in Fourier space, as described in section 4.

3. Coupled Model Description

The physical model that we use is the LFM global magnetosphere model coupled with the Rice Convection Model (RCM) [*Pembroke et al.*, 2012]. In accordance with equations equations (1) and (2), our methodology is to modify the pressure distribution in the inner magnetosphere such that the pattern of magnetic perturbations in the ionosphere matches optimally the one that we desire to reproduce. This is a natural extension of the coupling methodology of the LFM-RCM model, as well as of other models that couple global and inner magnetosphere components [*De Zeeuw et al.*, 2004; *Glocer et al.*, 2013].

Effectively, all such coupled models modify the plasma pressure—or, equivalently, the equation of state of the global model—in those regions in which the energy-dependent drifts play an important role. Assuming a linear relation between FAC currents $j_{\parallel}$ and magnetospheric pressure p in equation (1) and also assuming that all perturbations are linear, our methodology aims to weakly modify the plasma pressure after it is returned from the RCM but before it is inserted into the LFM.

The use of the LFM-RCM machinery considerably simplifies the implementation of this approach. As described in detail by *Pembroke et al.* [2012], in the RCM-to-LFM transfer step each grid cell in the LFM volume that happens to be located on a closed field line is traced back to the ionosphere, where it is assigned a pressure value from the RCM grid. Thus, the coupling machinery ensures that the magnetic field lines retain constant pressure in the coupled closed field region. This procedure allows us to avoid introducing spurious Alfvén waves into the simulation domain that might be caused by the pressure adjustment.

In this paper, we use the same LFM-RCM model version as described by *Pembroke et al.* [2012]. Therefore, we only mention here a few pertinent implementation details. The resolution of the LFM distorted spherical grid is $53 \times 48 \times 64$ cells, and the inner boundary is located at $2\ R_E$. The ionospheric solution is provided by the Magnetosphere-Ionosphere Coupler-Solver (MIX) of *Merkin and Lyon* [2010], while the RCM model is described in detail by *Toffoletto et al.* [2003].

4. Assimilation Procedure

Following the approach outlined in section 2, the assimilation procedure modifies the spatial 2-D distribution $\mathcal{P}$ of the plasma pressure p in the LFM-RCM simulation from the *background* $\mathcal{P}^{b}_{2D}$ to the *analysis* $\mathcal{P}^{a}_{2D}$, according to

$$\mathcal{P}^{a}_{2D} = \mathcal{P}^{b}_{2D} + \Delta\mathcal{P}. \tag{3}$$

We use here the unified notation for DA of *Ide et al.* [1997], and the pressure correction $\Delta\mathcal{P}$ is calculated by using the difference between the *observed* $\delta\mathbf{B}^{o}$ and the modeled background values $\delta\mathbf{B}^{b}$, where $\delta\mathbf{B}$ is the perturbation of the magnetic field from the ionospheric dipole field.

In the spirit of the Vasyliunas equation (1), we rely on a quasi-steady, linear approximation between $\mathcal{P}_{2D}$ and the ionospheric FACs. Hence, the required correction $\Delta\mathcal{P}$ is calculated by inverting the following linear system:

$$\delta\mathbf{B}^{o} - \delta\mathbf{B}^{b} = \mathbf{M}\Delta\mathcal{P}, \tag{4}$$

where $\mathbf{B}$ and $\mathcal{P}$ are numerically discretized fields; the subscript "2D" is hereafter omitted for brevity. For the general case of a rectangular matrix $\mathbf{M}$, the vector $\Delta\mathcal{P}$ in equation (4) is estimated by least squares minimization:

$$\Delta\mathcal{P} = \mathbf{R}_{pp}\mathbf{M}^{T}\left(\mathbf{M}\mathbf{R}_{pp}\mathbf{M}^{T} + \mathbf{R}_{BB}\right)^{-1}(\delta\mathbf{B}^{o} - \delta\mathbf{B}^{b}), \tag{5}$$

where $\mathbf{R}_{BB}$ and $\mathbf{R}_{pp}$ are error covariance matrices for $\delta\mathbf{B}$ and $\mathcal{P}$, respectively.

Note that the instantaneous differences between observed and modeled magnetic perturbations, $\delta\mathbf{B}^{o} - \delta\mathbf{B}^{b}$ in equation (4), will necessarily contain all spatial and temporal scales. To exclude transient and small-scale dynamics, our assimilation approach (section 2) focuses on large-scale and quasi-steady features of ionospheric FACs; hence, it necessitates a reduced-state representation that will rely here on scale-dependent decomposition of the magnetic and pressure fields to retain only the relevant dynamics. We adopted Fourier decomposition in space as the easiest filtering method to implement computationally and will consider only low-wave number modes of both magnetospheric pressure p and magnetic field $\delta\mathbf{B}$ while assuming that such modes capture well the quasi-static dynamics.

Following this reduced-state approach, the matrix $\mathbf{M}$ is estimated in Fourier space, and both $\delta\mathbf{B}$ and $\mathcal{P}$ are coefficients of the low-wave number Fourier modes from the respective spatial decompositions. Given our quasi-static, large-scale approximation, we can also reasonably assume that errors are contained in the fast and small scales, i.e., $\mathbf{R}_{BB} \approx 0$ for the large-scale Fourier modes of $\delta\mathbf{B}$, and that the resulting difference $\delta\mathbf{B}^{o} - \delta\mathbf{B}^{b}$ is solely due to large-scale magnetospheric pressure. When background errors of $\delta\mathbf{B}$ are neglected, i.e., $\mathbf{R}_{BB} \equiv 0$, equations (5) is formally equivalent to standard regression in order to find the optimal pressure correction $\Delta\mathcal{P}$:

$$\Delta\mathcal{P} = (\mathbf{M}^{T}\mathbf{M})^{-1}\mathbf{M}^{T}(\delta\mathbf{B}^{o} - \delta\mathbf{B}^{b}). \tag{6}$$

To summarize, the rectangular matrix $\mathbf{M}$ in equation (6) represents our quasi-steady, linear and reduced-state approximation (4) of the time-dependent, nonlinear MHD equations modeled by the LFM-RCM coupled code, and we estimate $\mathbf{M}$ numerically by introducing perturbations $\delta\mathbf{P}$ and calculating the response in ionospheric $\delta\mathbf{B}$, as described in the next section.

5. Numerical Implementation and Results

5.1. Details of the Numerical DA Algorithm

We start by constructing a baseline simulation into which we then assimilate the modified pressures. The coupled LFM-RCM code is run with idealized solar wind and IMF inputs: the solar wind velocity is constant in time, and it is purely antisunward, $V_x = -400$ km s^{-1}. Initial preconditioning of the magnetosphere used 2 h southward IMF, followed by 2 h northward IMF, with $|B_z| = 5$ nT, after which the IMF switched southward and remained constant at the value $B_z = -7.5$ nT for the remaining 12 h of the run. The plasma density was set equal to $n = 5$ cm^{-3} and the sound speed to $C_s = 40$ km s^{-1}. No dipole tilt was applied, and the ionospheric conductance $\boldsymbol{\Sigma}$ was held uniform and constant in time, with $\Sigma_P = 10$ S and $\Sigma_H = 0$ S for the Pedersen and Hall components, respectively. Because in our numerical experiments the Hall component of the conductance was always set equal to 0, the subscript P in Σ_P is hereafter omitted for brevity.

In the figures and in the discussion below, the simulation time (ST) is referenced to an arbitrary start time of 1 March 1995 0400 ST, such that the constant driving starts at 0800 ST. All assimilation tests and analysis are done after 6 h of constant driving, i.e., after 1400 ST. Figure 3 shows the resulting quasi-static configuration of the FACs. Like in the results of *Pembroke et al.* [2012], both large-scale R1 and R2 current systems are evident in the figure and include the typical two-cell convection pattern and effective shielding of the electric field at lower latitudes. Some smaller-scale features in the currents can also be seen on the nightside. In this work, we will only consider larger-scale structures, as described below.

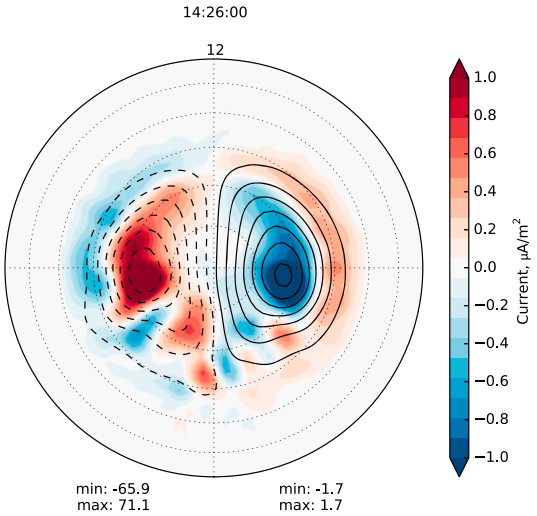

Figure 3. A snapshot of the baseline LFM-RCM simulation ($\Sigma = 10$ S) during the quasi-steady stage of the simulation (time indicated at the top). The Northern Hemisphere FACs including both R1 and R2 currents are shown. Upward current is positive. Solar magnetic coordinates are used such that the pole coincides with the Earth's magnetic axis, and noon is at the top. The distance between the constant latitude circles is 10°. The corresponding ionospheric potential is indicated by black contours (solid = positive and dashed = negative). The contours are spaced by roughly 10 kV. Minimum/maximum values for the current density and potential are indicated in the bottom right and left corners, correspondingly.

To implement the assimilation procedure described in section 4, one needs to perform Fourier transforms of both the magnetic field **B** and the magnetospheric pressure $\mathcal{P}$, as well as estimate the linear approximation matrix **M**. Computing **M** amounts to quasi-steady linearization of the full, time-dependent nonlinear MHD equations of the LFM-RCM code, and it cannot be explicitly obtained from the numerical code. In order to estimate **M**, we adopt a procedure sometimes used in oceanographic DA [*Fukumori*, 2006], as well as in many other applications in which—due to the complexity of the numerical scheme—the discretized dynamical equations are not available explicitly in matrix form. Hence, the latter form has to be computed by numerical perturbations, as described below.

First, we perform spatial Fourier transforms of instantaneous magnetospheric pressure and spherical magnetic field components $\delta B = (\delta B_\phi, \delta B_\theta)$ at the inner boundary (2 R_E) of the baseline simulation and obtain the Fourier coefficients $\{P^b_n : n = 1, \ldots, N\}$ and $\{\delta B^b_i : i = 1, .., I\}$ of the large-scale modes to be retained in our analysis. Next, we consider the difference between the LFM-RCM baseline simulation, in which only the large-scale modes are retained, referred to hereafter as "background," and the model run in which the Fourier mode n_0 of the magnetospheric pressure is perturbed, i.e., $\mathcal{P}^* = (P^b_1, \ldots., P^b_{n_0} + \delta P, \ldots P^b_N)$.

Given the Fourier coefficients $\{\delta B^*_i : i = 1, \ldots, I\}$ of the large-scale modes of the magnetic field components in the perturbed run, one estimates the ith element in the n_0th column of the matrix **M** by

$$M_{i,n_0} = \frac{\delta B^*_i - \delta B^b_i}{\delta P}. \tag{7}$$

Because the estimation of the $N \times I$ matrix **M** can be performed for arbitrary spatial distributions of background equatorial pressure and magnetic field, our assimilation procedure is not restricted to a particular configuration of field-aligned currents or solar driver values.

We have considered $K = 18$ radial locations in the ionospheric region $0.4 < R < 0.58\ R_E$, in which the RCM pressure is localized. Figure 4a shows the RCM pressure distribution, on its ionospheric grid, corresponding to the FAC pattern in Figure 3. For each of these radial locations, we performed a Fourier transform along the azimuthal direction and computed the corresponding Fourier coefficients for the modes with wave numbers $j = 0, .., J$. For each of the radial locations and the azimuthal modes with wave number $j > 0$, we consider $L = 2$ types of perturbations, $\delta\mathcal{P}_j(1)$ and $\delta\mathcal{P}_j(2)$, shifted by $\pi/2$ and orthogonal to each other. This is equivalent to an independent perturbation of the real and imaginary parts of the respective Fourier transform. On the other hand, for the azimuthally uniform mode with wave number $j = 0$, the imaginary part of each Fourier coefficient is identically 0, and so there is only one perturbation to consider.

We also note that azimuthally symmetric modes of the pressure field do not generate a significant FAC since their pressure gradient is largely aligned with the gradient of the flux tube volume. Moreover, we

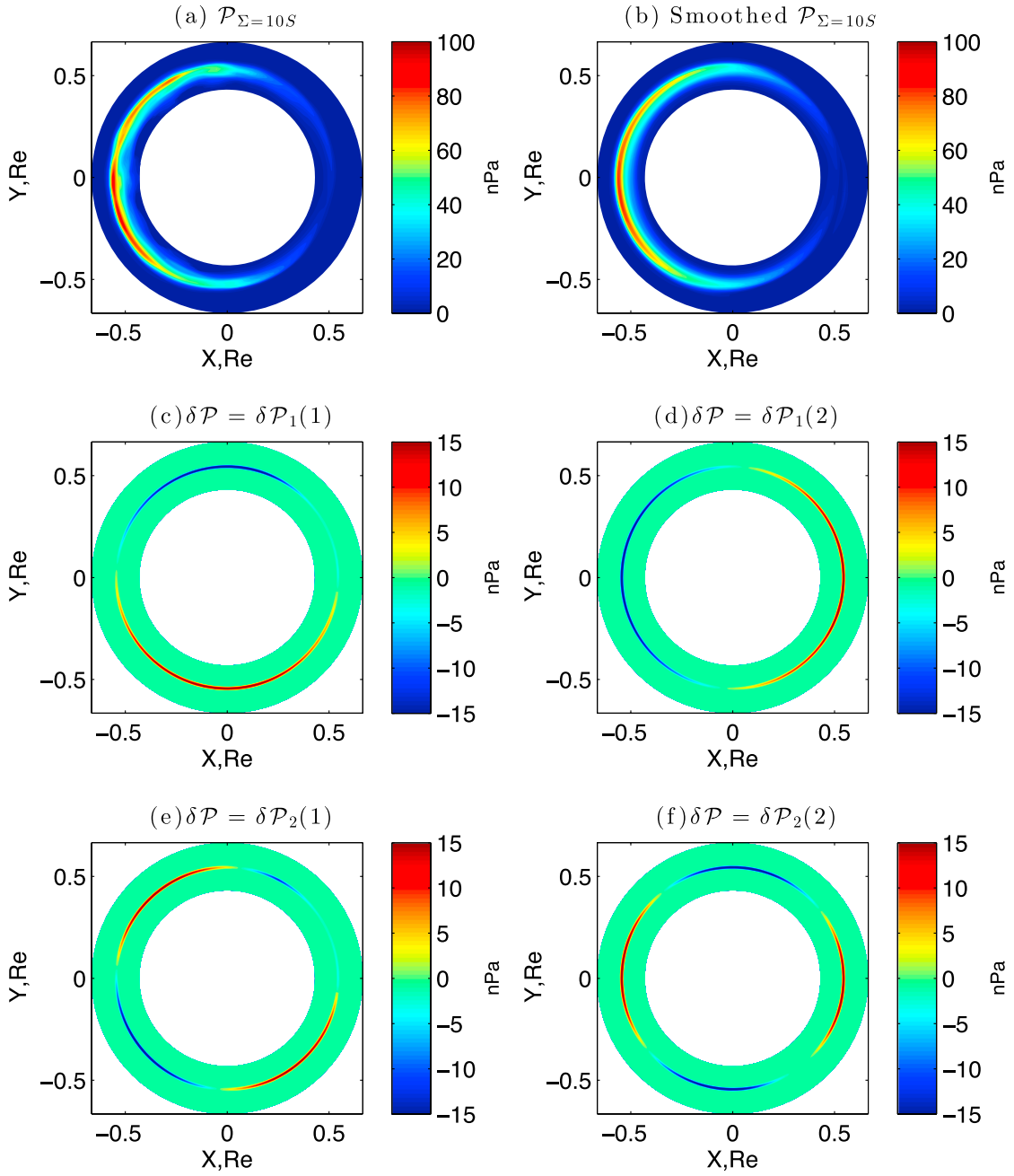

Figure 4. RCM pressure fields used in our DA algorithm, shown on the RCM's ionospheric grid. Time corresponds to Figure 3, i.e., 1426 ST. (a) Full and (b) Fourier-smoothed pressure (nPa) in the coupled model's background solution. (c–f) Numerical perturbations δP_j of $j = 1, 2$ azimuthal wave number modes that are applied at $R = 0.54\ R_E$ in order to compute the model matrix **M** in equation (7). For each wave number j, two types of perturbations $\delta P_j(1)$ and $\delta P_j(2)$ are considered: the two are shifted by $\pi/2$ and are orthogonal to each other.

found that the most effective large-scale response in FACs was generated by pressure perturbations in the $K_R = 5$ radial locations located in the smaller region around the pressure maximum, i.e., $R/R_E = 0.5213, 0.5306, 0.5400, 0.5495, 0.5591$.

Furthermore, our experiments have shown that perturbations of azimuthal modes with wave number larger than $J = 2$ were not effective in generating a significant large-scale FAC response. Figure 4b shows the same distribution as in Figure 4a but only retaining the $j = 0–2$ modes. Figures 4c–4f, in turn, show the structure

of the $j = 1, 2$ pressure perturbations for $R/R_E = 0.54$. Accordingly, we have restricted the total number of perturbed pressure runs for estimating **M** via equation (7) to $N = K_R \times J \times L + K_R = 25$. The second term in N accounts for perturbations of the $j = 0$ azimuthal mode, and it was kept only for illustrative purposes, as it does not generate significant FACs.

For $\delta\mathbf{B} = (\delta B_\phi, \delta B_\theta)$ we performed a 2-D Fourier decomposition of each spherical component in both latitude and longitude and kept the modes up to wave number 3, which were found to be most robust and energetic in response to applied pressure perturbations. Including both the real and imaginary parts of the Fourier transform for $\delta\mathbf{B}$, this truncation amounts to a total of $I = 98$ coefficients that we need to estimate for **M** via equation (7). Note that the number $N \times I = 25 \times 98 = 2450$ of scalars retained in this reduced-state representation is much smaller than the total number of degrees of freedom in the numerically discretized fields, since the latter equals $40 \times 100 = 4000$ for the RCM pressure in the region of interest plus $2 \times 32 \times 48 = 3072$ for two spherical components of the magnetic field $\delta\mathbf{B}$.

Figure 4 illustrates how our low-wave number smoothing procedure by truncated Fourier transform does effectively discard small scales and emphasizes quasi-steady large-scale features. The perturbation was applied on the RCM ionospheric grid and then used to nudge the LFM over the exchange time interval of 1 min, as described by *Pembroke et al.* [2012]. We randomly selected 1425 ST as the time when starting to apply the perturbed pressure nudging of the LFM solution. The perturbed pressure was kept constant for 5 min to allow the system to adjust and reach a new quasi-steady state.

Figures 5–8 demonstrate the resulting differences between the background simulation and the perturbed LFM-RCM runs. Since we only adjusted the inner magnetosphere pressure, solely R2 currents in the ionosphere responded to the perturbations, as is clear from Figures 5c, 6c, 7c, and 8c. Furthermore, the responses in the coupled model's pressure field in both the equatorial (Figures 5a, 6a, 7a, and 8a) and meridional (Figures 5b, 6b, 7b, and 8b) planes, as well as of the ionospheric FACs (Figures 5c, 6c, 7c, and 8c), are largely governed by the spatial shape and wave number of the applied perturbations. This finding is entirely consistent with the assumed linear approximation of equation (4), and it is further emphasized by the potential contours in Figures 5c, 6c, 7c, and 8c, which outline the spatial structure of the current perturbations.

Note that the color scales of the pressure perturbations in Figures 5a, 5b, 6a, 6b, 7a, 7b, 8a, and 8b are limited to ± 1 nPa. This narrow range may suggest that the amplitude of pressure perturbations has been reduced by an order of magnitude after being gradually inserted into the LFM. However, this is not the case as the scales have been deliberately saturated to bring out the mode structure in the pressure difference between the background and perturbed simulations. The perturbations on the RCM grid have the amplitude of 10% of the RCM pressure peak (cf. Figure 4), i.e., approximately 10 nPa. When gradually inserted into the LFM model, the peak pressure is indeed attenuated somewhat, possibly because of the differences in grid resolution between the LFM and the RCM, and so is the amplitude of pressure perturbations. But this attenuation is no more than roughly 40% of the peak pressure, not a factor of 10. The perturbation in the current density (Figures 5c, 6c, 7c, and 8c) relative to the background (Figure 3) may be further attenuated, but the effect is not dramatic.

Because FACs are generated predominately by the azimuthal pressure gradient, the perturbation in the currents is out of phase with the perturbation in the pressure. This out-of-phase relation is clearly seen in all of Figures 5–8; see Figures 5a, 6a, 7a, and 8a versus Figures 5c, 6c, 7c, and 8c. The pressure perturbations in the noon-midnight meridional plane in Figures 5b and 7b are almost nonexistent because the azimuthal perturbation has a node there, cf. Figures 5a and 7a. On the other hand, Figures 6b and 8b show the pressure perturbations distributed over flux tubes from the equator to the ionosphere, as expected from our quasi-equilibrium-based algorithm and from the azimuthal structure of these modes; see Figures 6a and 8a.

Note that the pressure perturbations applied by our DA algorithm may cause total pressure to drop below zero where $\mathcal{P}$ has low values. This nonphysical artifact was removed simply by zeroing out the perturbation in such regions, such as for $\delta P_2(1)$ in Figure 4c.

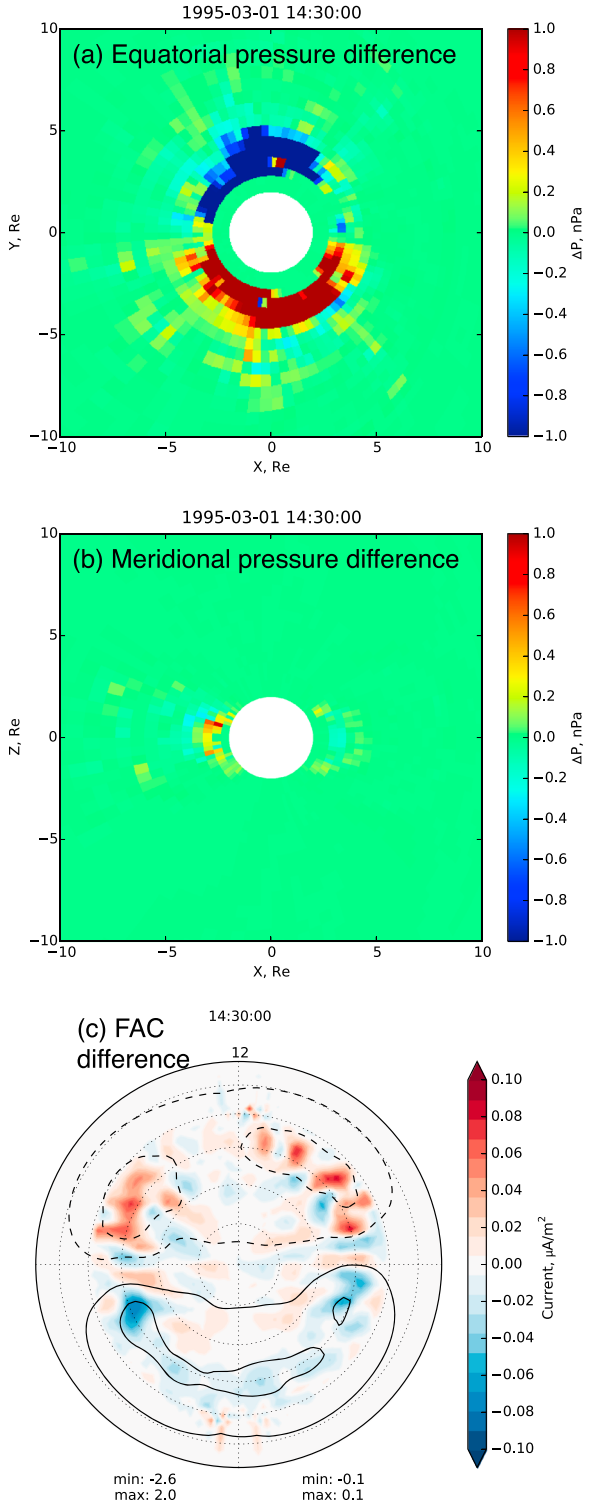

Figure 5. Magnetospheric and ionospheric responses to the $\delta P = \delta P_1(1)$ perturbation in Figure 4c. LFM (a) equatorial and (b) meridional pressure differences between the background and perturbed runs; (c) Northern Hemisphere FAC and potential response indicated by a difference between the background and perturbed runs. The format of the dial plot is the same as in Figure 3a, except that the color scale is reduced by a factor of 10 and the distance between potential contours is approximately 1 kV.

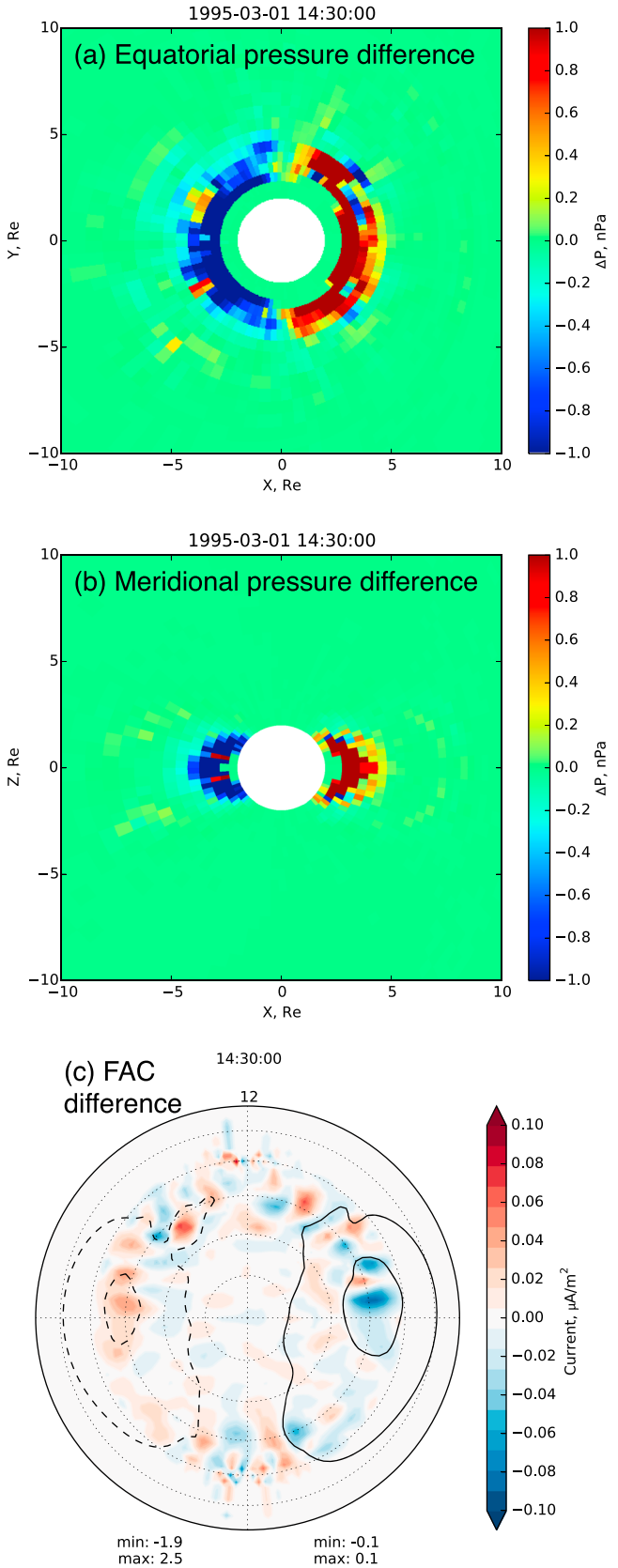

Figure 6. Magnetospheric and ionospheric responses to the $\delta P = \delta P_1(2)$ perturbation in Figure 4d. Same layout as in Figure 5.

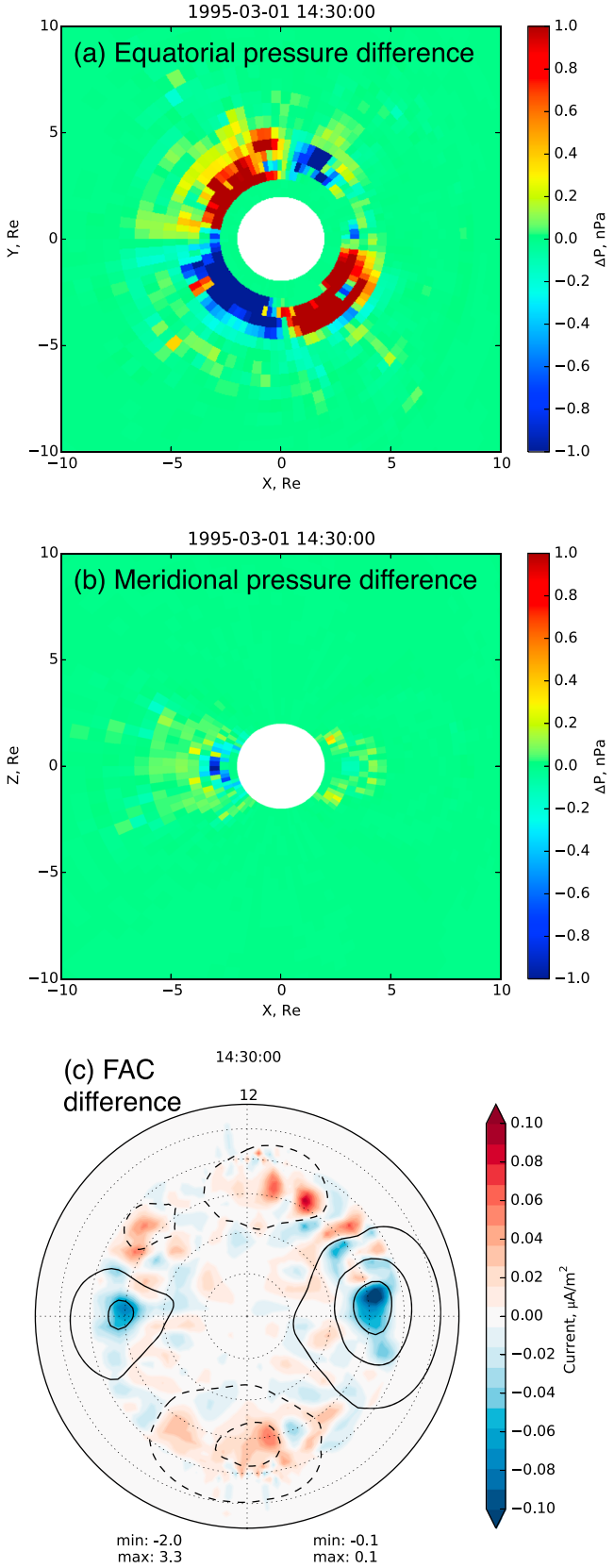

Figure 7. Magnetospheric and ionospheric responses to the $\delta P = \delta P_2(1)$ perturbation in Figure 4e. Same layout as in Figure 5.

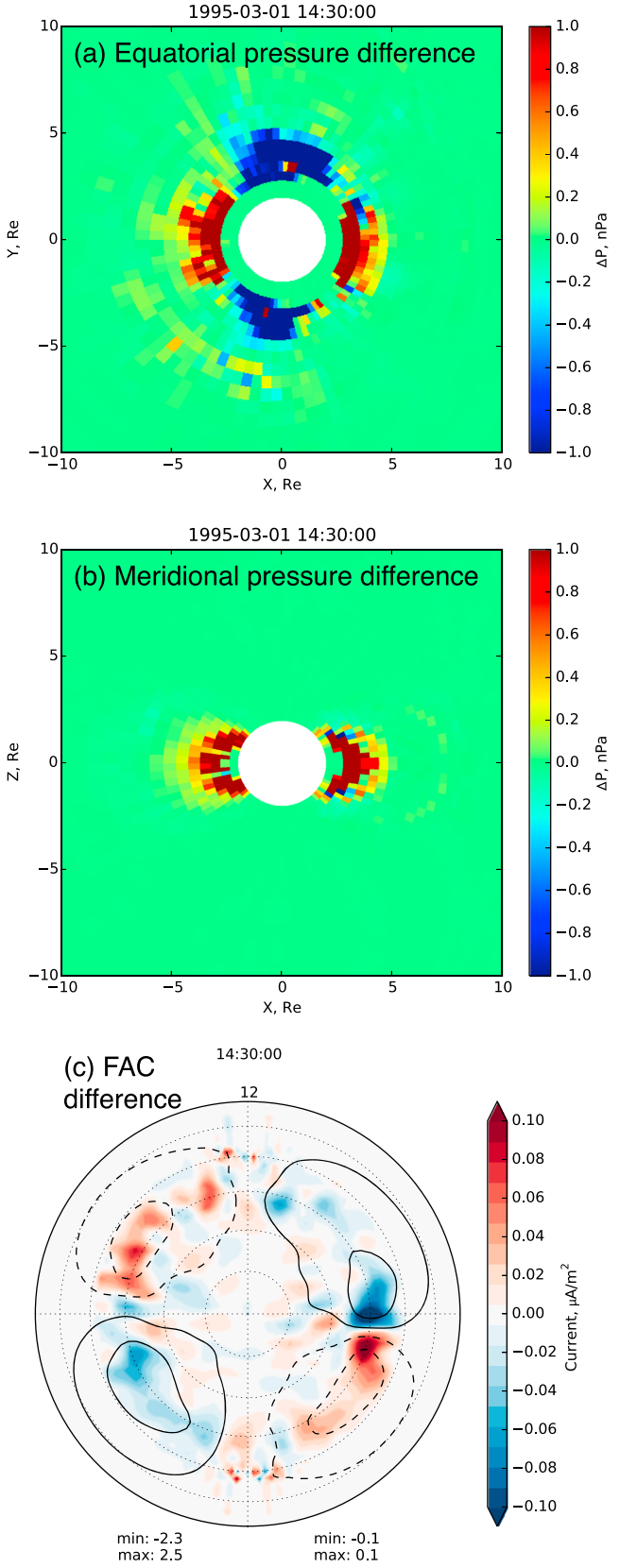

Figure 8. Magnetospheric and ionospheric responses to the $\delta P = \delta P_2(2)$ perturbation in Figure 4f. Same layout as in Figure 5.

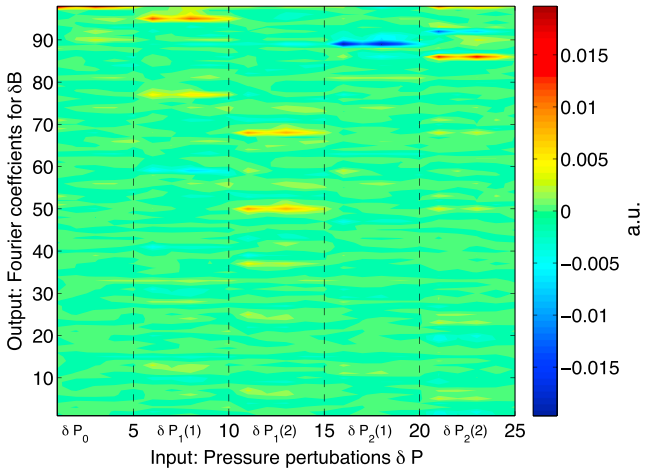

Figure 9. The reduced-state model's matrix **M** for perturbations of equatorial pressure δP and response in magnetic field $\delta\vec{\mathbf{B}} = (\delta B_\phi, \delta B_\theta)$. This rectangular matrix has dimensions $N \times I = 28 \times 95$.

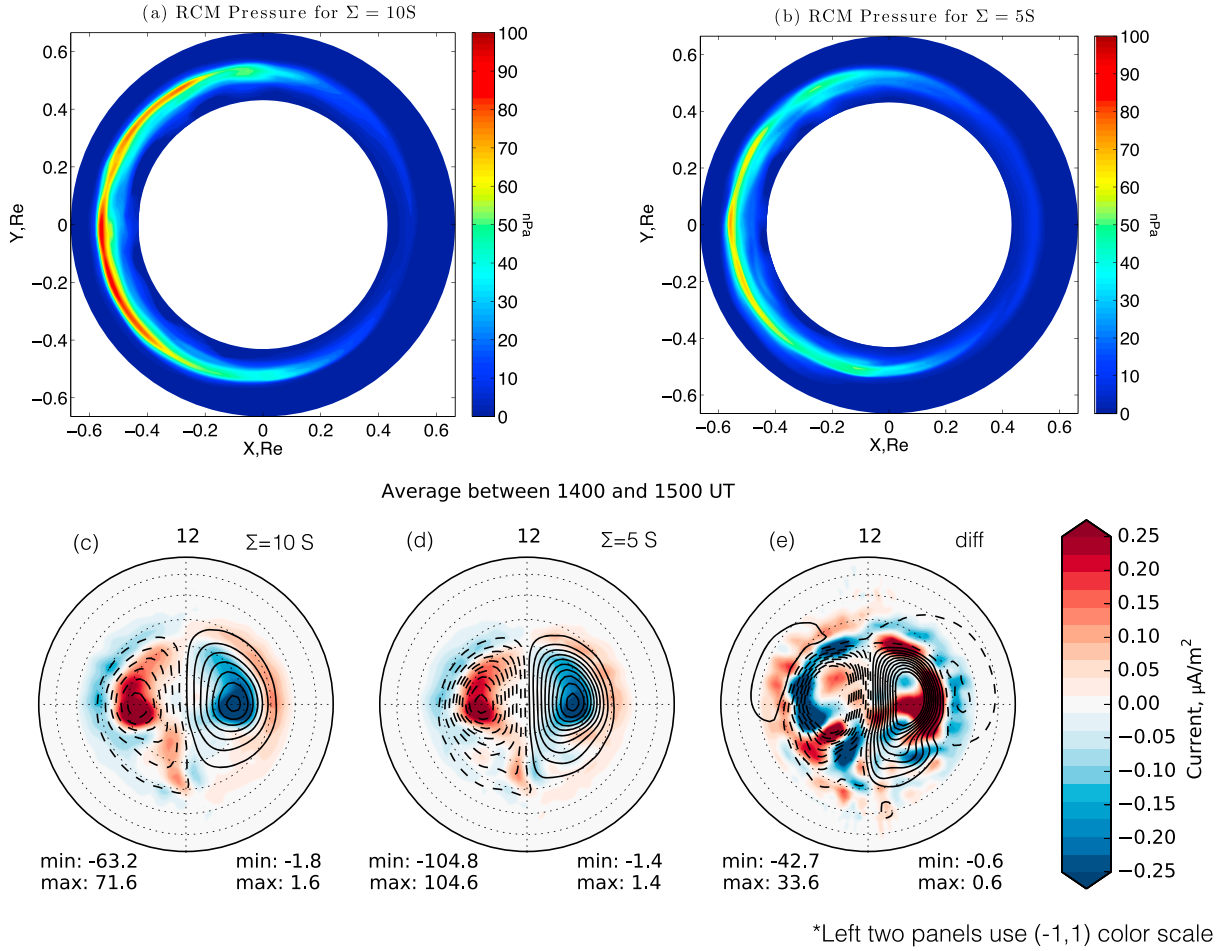

Figure 10. The experimental setup of *fraternal twins* for testing our assimilation procedure. The magnetic perturbations from the control model solution with ionospheric conductance $\Sigma = 5$ S are assimilated into the background simulation with conductance $\Sigma = 10$ S aiming to correct the imperfect model by the observed difference in FACs. Instantaneous (1426 ST) RCM pressure (a) for the baseline run, with $\Sigma = 10$ S (same as Figure 4a), and (b) for the control run, $\Sigma = 5$ S. (c, d) FACs and potentials for the same runs averaged between 1400 and 1500 ST to minimize transient differences. (e) The difference between the FACs and potentials in Figures 10d and 10c. The format of the dial plots in Figures 10c and 10d is the same as in Figure 3. Note that Figures 10c and 10d use the same color scale as Figure 10e but with (−1, 1) limits. Potential contour separation is approximately 10 kV in Figures 10c and 10d and 2.5 kV in Figure 10e.

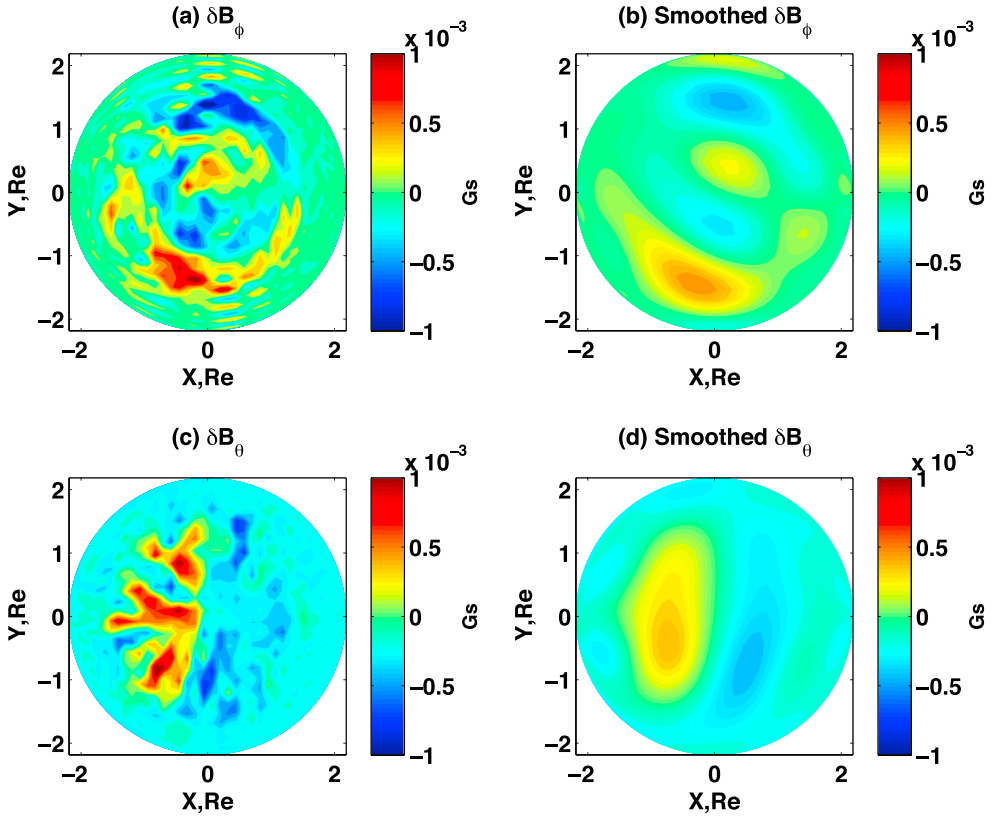

Figure 11. The instantaneous difference in the ionospheric magnetic perturbations between the control ($\Sigma = 5$ S) and baseline ($\Sigma = 10$ S) runs at 1426 ST. (a) δB_ϕ and (c) δB_θ; (b, d) the smoothed versions of δB_ϕ and δB_θ. The large-scale features of the Fourier-smoothed field correspond to the FAC pattern in Figure 10e and are used by our assimilation procedure to estimate the equatorial pressure correction for the coupled LFM-RCM model, via equation (6).

The rectangular, 25×98 matrix **M** is plotted in Figure 9, and it is clear from this plot that pressure perturbations in the same azimuthal mode applied at different radial locations lead to a very similar response in δ**B**. This strong degeneracy in **M** is most likely explained by the predominant FAC generation by azimuthal pressure gradients, in combination with the low LFM resolution used in the simulations presented here: in fact, the entire RCM pressure peak fits radially into a few LFM grid cells.

To remove this degeneracy requires one to regularize the solution of equation (6). We opted to do so by using principal component regression [*Hastie et al.*, 2009] by carrying out a singular value decomposition (SVD) of **M** and retaining only six leading SVD modes.

5.2. Numerical Results for Synthetic Data

To validate our assimilation procedure, we perform the following "fraternal twin" model experiments with synthetic data, whereby the *control* simulation by the same model but with different parameter values is used to obtain synthetic observations [*Ghil and Malanotte-Rizzoli*, 1991; *Kalnay*, 2006; *Kondrashov et al.*, 2011]. To this end, as our control simulation, we have used LFM-RCM with $\Sigma = 5$ S in the ionosphere but otherwise identical to the background run. The magnetic perturbations from the fraternal twin control simulation with $\Sigma = 5$ S in the ionosphere are then assimilated into the background simulation with $\Sigma = 10$ S, aiming to correct both the pressure distribution and the R2 FACs of the imperfect model.

Figure 10 compares the synthetic observations and the baseline simulation, i.e., $\Sigma = 5$ S versus $\Sigma = 10$ S. Figures 10c–10e confirm that lower conductance results in weaker FACs, which global MHD simulations have shown to be the case for at least the R1 current system [e.g., *Fedder and Lyon*, 1987; *Merkin et al.*, 2005], and observations have confirmed as well [*Ohtani et al.*, 2014]. Figure 10 now demonstrates that both R1 and R2 are affected due to the conductance decrease. Note that the differences in Figure 10e are due to changes in magnitude of the currents as well as their spatial displacement.

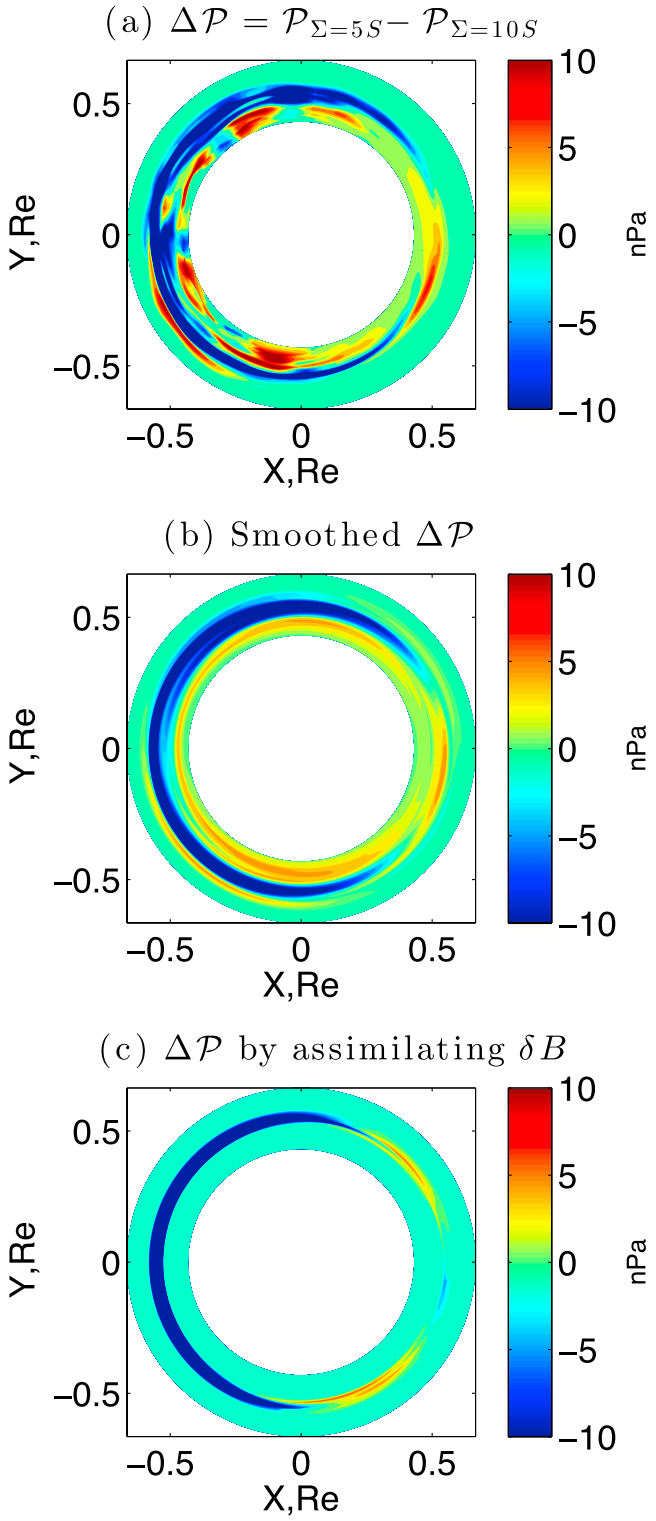

Figure 12. Differences $\Delta\mathcal{P}$ in the RCM pressure (nPa) for our fraternal twins experiment, as defined in Figure 10. (a) Pressure difference $\Delta\mathcal{P} = \mathcal{P}^{o} - \mathcal{P}^{b}$ between the synthetic observations and the background simulation, (b) smoothed version of the $\Delta\mathcal{P}$ in Figure 12a above, and (c) pressure correction for the LFM-RCM model calculated by our DA procedure. The latter reproduce the Fourier-smoothed true difference in Figure 12b above at the lower latitudes where the DA procedure is applied.

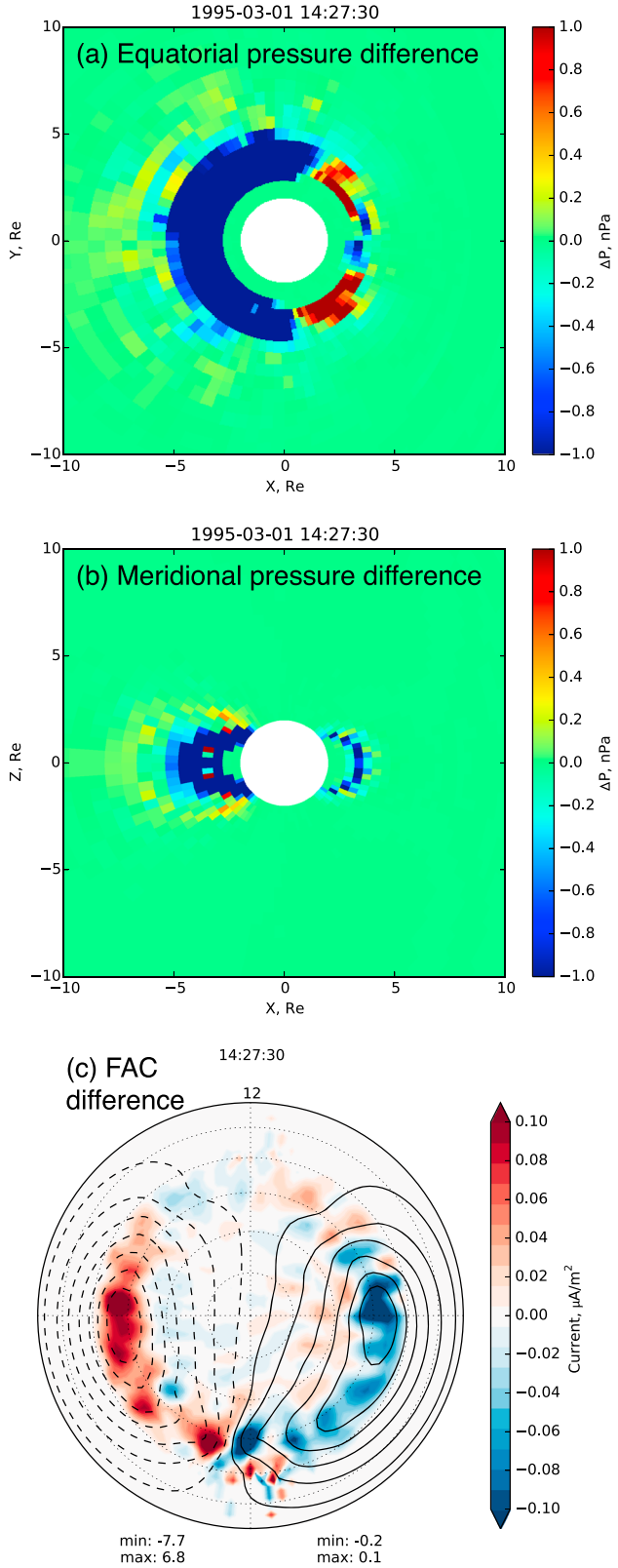

Figure 13. Response of the background LFM-RCM simulation with $\Sigma = 10$ S to the pressure corrections applied by the proposed DA procedure. Same layout as in Figures 5–8. The large-scale dipolar pattern of both the equatorial pressure and the R2 FACs is qualitatively similar to the observed difference between the synthetic observations and the background simulation, as shown in Figure 10e.

Moreover, Figures 10a and 10b reveal that the inner magnetosphere pressure distribution also adjusts accordingly, so as to reduce the pressure maximum and, correspondingly, its azimuthal gradient. This reduction is consistent with weaker R2 currents in the ionosphere, cf. Figure 10e. Accordingly, our assimilation procedure will aim to reduce the currents in the background simulation with the higher conductance and bring it closer to the synthetic observations generated by the fraternal twin model with the lower conductance. By design of the experiment, we only expect a response in the large-scale spatial modes of the R2 current system alone.

The corresponding difference between synthetic observations $\delta\mathbf{B}^{o}$ and the model $\delta\mathbf{B}^{b}$ is shown in Figure 11, where the Fourier-smoothed field in Figures 11b and 11d is dominated by large-scale spatial features that correspond to the negative-positive (dawn-dusk) azimuthal FAC R2 pattern in Figure 10e. The pressure correction $\Delta\mathcal{P}$ in Fourier space can then be readily obtained via equation (6), with the matrix **M** estimated from equation (7).

Figure 12 compares three distinct ways of calculating differences $\Delta\mathcal{P}$ between the synthetic observations of equatorial pressure and those of the coupled LFM-RCM model. Figure 12c shows that—when $\Delta\mathcal{P}$ is transformed back to physical space—it largely reproduces, as expected, the large-scale features of the Fourier-smoothed "true" difference in the equatorial pressure between the observations and the background simulation, cf. Figures 12a and 12b, except for the high-latitude regions that were excluded from our DA procedure.

Finally, $\Delta\mathcal{P}$ obtained in the analysis step [*Ghil and Malanotte-Rizzoli*, 1991; *Ide et al.*, 1997; *Kalnay*, 2006, and references therein] via equation (6) is inserted into the background LFM-RCM version with $\Sigma = 10$ S to verify that the imperfect model is indeed nudged closer to the observations by our DA approach. The $\Delta\mathcal{P}$ is inserted by the LFM-RCM coupling scheme at each grid point of the RCM ionospheric grid in the same way as was used to calculate the model matrix **M** by the perturbation method.

The insertion starts at 1425 ST, and we plot the result 2.5 min later in Figure 13. The pressure corrections are distributed over the entire flux tubes in Figure 13b, ensuring that the system remains in quasi-equilibrium and affecting magnetic perturbations immediately at low altitudes.

The analysis-model difference in the FAC system, after applying the correction $\Delta\mathcal{P}$, is plotted in Figure 13. The resulting dipolar pattern qualitatively agrees with the observations-model difference, as shown in Figure 10, although the magnitude in the former is underestimated. By our experimental design, only the R2 currents are modified and these have been reduced in magnitude on both the dawn and dusk sides. This effect is less pronounced on the dayside than in Figure 10e, which was suggested already by the differences in pressure distributions in Figures 12c and 12b. Note that the potential leaking to latitudes equatorward of the R2 currents—which is due to their weakening relative to the background run—has a different sign in Figures 10e and 13c. This sign change is an effect of R1 current changes evident in Figure 10e but unaccounted for in our assimilation experiment.

In summary, we achieved the desired outcome of our assimilation procedure; i.e., FACs in the imperfect LFM-RCM model's R2 region were nudged closer to the synthetic observations by the proposed assimilation procedure.

6. Summary and Conclusion

We have described an approach to develop methods for the assimilation of ionospheric magnetic perturbations into global magnetosphere models. This work was motivated by the emergence of global ionospheric data sets such as AMPERE [*Anderson et al.*, 2014], which combines observations from the Iridium satellite constellation. The ionosphere is the region of geospace where such global in situ measurements are feasible and are already available in fact. In addition, remote global measurements of ground-based magnetic perturbations and of ionospheric convection are also available from SuperMAG [*Gjerloev*, 2012] and Super Dual Auroral Radar Network [e.g., *Chisham et al.*, 2007], respectively, and these could also be assimilated.

In this paper, we concentrated on the idea that ionospheric magnetic perturbations associated with field-aligned currents (FACs) can be assimilated by adjusting their generator in the magnetosphere. In particular, the Region 2 current system is well suited for this approach because these currents are generated by the quasi-steady pressure distribution in the inner magnetosphere and thus one can deal, at least initially,

with slow time scales and large spatial scales. Focusing on slow time scales means that we assume the system to be in equilibrium and, in particular, the isotropic plasma pressure to be constant along magnetic field lines. Large spatial scales mean that we consider only long azimuthal wavelengths, effectively smoothing out mesoscale structures that span 6 h in MLT or less, e.g., magnetic field dipolarizations and high-speed channels.

We used the coupled LFM-RCM magnetosphere-ionosphere model [*Pembroke et al.*, 2012, and references therein] and calculated the model matrix **M** by applying a perturbation technique in Fourier space. To test the method, we relied in this paper on synthetic data generated by an LFM-RCM run with a lower ionospheric conductance but identical otherwise. We ran the model for 5 min with the synthetic data being assimilated to confirm that it responded correctly by modifying ionospheric currents and magnetic perturbations so as to nudge them toward consistency with the synthetic observations. We thus found the approach proposed herein to be promising for future assimilation of real data.

However, there are a number of important steps that need to be taken first. In this paper we have only tested our approach within one assimilation cycle. Clearly, more tests and longer simulations are needed to ensure code stability and convergence toward the observed state over longer time intervals. The assimilation procedure effectively assumes that the system response to perturbations is linear. Thus, investigation of nonlinear feedback loops over several assimilation cycles will be of significant interest.

Furthermore, although the response of the coupled model to assimilating synthetic data demonstrated the correct trend, i.e., the ionospheric current decreased when the ionospheric conductance was reduced, this response was underestimated by at least a factor of 2–3. The reasons for the weak response will need to be investigated in future studies, in particular the effects of simulation resolution and biases. An imperfect model will tend to drift away from the analysis state, but if large-scale, quasi-steady FAC distribution is maintained in observations, additional assimilation cycles will necessarily improve the analysis further.

In general, a similar approach should be taken for other FAC generators and controlling parameters, e.g., variation of solar wind drivers for the R1 region and ionospheric conductance. Eventually, assimilation should be based on such optimization approaches—whether variational or statistical [*Ghil and Malanotte-Rizzoli*, 1991]—that are applied to all relevant variables in concert. In addition, the reduced-space representation of the assimilation methodology need not be restricted to the truncated Fourier transform used herein: it can easily be adapted for other practical decompositions—such as spherical cap harmonics used to obtain global distribution of currents in the AMPERE procedure or more sophisticated methods that work in a dynamically active subspace [*Carrassi et al.*, 2008].

Acknowledgments
We would like to thank K. Baker for his encouragement and interest in this project. V.G.M. would also like to thank F. Toffoletto at Rice University for the use of the RCM-to-LFM transfer algorithm and to acknowledge fruitful discussions with M.I. Sitnov at JHU/APL. This research was supported by National Science Foundation (NSF) grant AGS-12420122. V.G.M. additionally acknowledges NASA grant NNX16AB80G. AMPERE is supported under NSF grant AGS-1420184. We would like to acknowledge high-performance computing support from the IBM iDataPlex cluster Yellowstone, provided by NCAR's Computational and Information Systems Laboratory and sponsored by the NSF. The data used to produce figures, animations, and analysis in the paper are available upon request.

References

Anderson, B. J., K. Takahashi, and B. A. Toth (2000), Sensing global Birkeland currents with Iridium® engineering magnetometer data, *Geophys. Res. Lett.*, *27*(24), 4045–4048.

Anderson, B. J., H. Korth, C. L. Waters, D. L. Green, V. G. Merkin, R. J. Barnes, and L. P. Dyrud (2014), Development of large-scale Birkeland currents determined from the Active Magnetosphere and Planetary Electrodynamics Response Experiment, *Geophys. Res. Lett.*, *41*(9), 3017–3025.

Bengtsson, L., M. Ghil, and E. Källén (1981), *Dynamic Meteorology: Data Assimilation Methods*, Springer, New York.

Carrassi, A., M. Ghil, A. Trevisan, and F. Uboldi (2008), Data assimilation as a nonlinear dynamical systems problem: Stability and convergence of the prediction-assimilation system, *Chaos*, *18*(2), 023112.

Chisham, G., et al. (2007), A decade of the Super Dual Auroral Radar Network (SuperDARN): Scientific achievements, new techniques and future directions, *Surv. Geophys.*, *28*, 33–109, doi:10.1007/s10712-007-9017-8.

Daley, R. (1996), *Atmospheric Data Analysis*, Cambridge Atmospheric and Space Science Series, Cambridge Univ. Press.

De Zeeuw, D. L., S. Sazykin, R. A. Wolf, T. I. Gombosi, A. J. Ridley, and G. Tóth (2004), Coupling of a global MHD code and an inner magnetospheric model: Initial results, *J. Geophys. Res.*, *109*, A12219, doi:10.1029/2003JA010366.

Evensen, G. (2003), The ensemble Kalman filters: Theoretical formulation and practical implementation, *Ocean Dyn.*, *53*, 343–367.

Fedder, J. A., and J. G. Lyon (1987), The solar wind-magnetosphere-ionosphere current-voltage relationship, *Geophys. Res. Lett.*, *14*, 880–883.

Fukumori, I. (2006), What is data assimilation really solving, and how is the calculation actually done?, in *Ocean Weather Forecasting: An Integrated View of Oceanography*, edited by E. P. Chasignet and J. Verron, Springer, Netherlands.

Ghil, M., and S. Childress (2009), Topics in geophysical fluid dynamics: Atmospheric dynamics, dynamo theory and climate dynamics.

Ghil, M., and P. Malanotte-Rizzoli (1991), Data assimilation in meteorology and oceanography, *Adv. Geophys.*, *33*, 141–266.

Gjerloev, J. W. (2012), The SuperMAG data processing technique, *J. Geophys. Res.*, *117*(A9), A09213, doi:10.1029/2012JA017683.

Glocer, A., M. Fok, X. Meng, G. Toth, N. Buzulukova, S. Chen, and K. Lin (2013), CRCM+BATSRUS two-way coupling, *J. Geophys. Res.*, *118*(4), 1635–1650, doi:10.1002/jgra.50221.

Godinez, H. C., and J. Koller (2012), Localized adaptive inflation in ensemble data assimilation for a radiation belt model, *Space Weather*, *10*, S08001, doi:10.1029/2012SW000767.

Hastie, T., R. Tibshirani, and J. Friedman (2009), *The Elements of Statistical Learning: Data Mining, Inference, and Prediction*, 2nd ed., Springer Series in Statistics.

Ide, K., P. Courtier, M Ghil, and A. Lorenc (1997), Unified notation for data assimilation: Operational, sequential and variational, *J. Meteorol. Soc. Japan*, *75*, 181–189.
Iijima, T., and T. A. Potemra (1976), Field-aligned currents in the dayside cusp observed by Triad, *J. Geophys. Res.*, *81*(34), 5971–5979.
Iijima, T., and T. A. Potemra (1978), Large-scale characteristics of field-aligned currents associated with substorms, *J. Geophys. Res.*, *83*(A2), 599–615.
Janhunen, P., M. Palmroth, T. Laitinen, I. Honkonen, L. Juusola, G. Facskó, and T. I. Pulkkinen (2012), The GUMICS-4 global MHD magnetosphere-ionosphere coupling simulation, *J. Atmos. Sol. Terr. Phys.*, *80*, 48–59, doi:10.1016/j.jastp.2012.03.006.
Kalnay, E. (2006), *Atmospheric Modeling, Data Assimilation and Predictability*, 3rd ed., Cambridge Univ. Press, Cambridge, U. K.
Koller, J., Y. Chen, G. D. Reeves, R. H. W. Friedel, T. E. Cayton, and J. A. Vrugt (2007), Identifying the radiation belt source region by data assimilation, *J. Geophys. Res.*, *112*(A6), A06244, doi:10.1029/2006JA012196.
Kondrashov, D., Y. Shprits, M. Ghil, and R. Thorne (2007), A Kalman filter technique to estimate relativistic electron lifetimes in the outer radiation belt, *J. Geophys. Res.*, *112*(A10), A10227, doi:10.1029/2007JA012583.
Kondrashov, D., M. Ghil, and Y. Shprits (2011), Log-normal Kalman filter for assimilating phase-space density data in the radiation belts, *Space Weather*, *9*, S11006, doi:10.1029/2011SW000726.
Lapenta, G. (2012), Particle simulations of space weather, *J. Comp. Phys.*, *231*(3), 795–821, doi:10.1016/j.jcp.2011.03.035.
LeBoeuf, J. N., T. Tajima, C. F. Kennel, and J. M. Dawson (1978), Global simulation of the time-dependent magnetosphere, *Geophys. Res. Lett.*, *5*(7), 609–612, doi:10.1029/GL005i007p00609.
Liemohn, M. W., J. U. Kozyra, C. R. Clauer, and A. J. Ridley (2001), Computational analysis of the near-Earth magnetospheric current system during two-phase decay storms, *J. Geophys. Res.*, *106*(A12), 29,531–29,542.
Lopez, R. E., V. G. Merkin, and J. G. Lyon (2011), The role of the bow shock in solar wind-magnetosphere coupling, *Ann. Geophys.*, *29*(6), 1129–1135.
Lyon, J., S. Brecht, J. Huba, J. Fedder, and P. Palmadesso (1981), Computer simulation of a geomagnetic substorm, *Phys. Rev. Lett.*, *46*(15), 1038–1041, doi:10.1103/PhysRevLett.46.1038.
Lyon, J. G., J. A. Fedder, and C. M. Mobarry (2004), The Lyon-Fedder-Mobarry (LFM) global MHD magnetospheric simulation code, *J. Atmos. Sol. Terr. Phys.*, *66*, 1333–1350, doi:10.1016/j.jastp.2004.03.020.
Matsuo, T., D. J. Knipp, A. D. Richmond, L. Kilcommons, and B. J. Anderson (2015), Inverse procedure for high-latitude ionospheric electrodynamics: Analysis of satellite-borne magnetometer data, *J. Geophys. Res.*, *120*(6), 5241–5251, doi:10.1002/2014JA020565.
Merkin, V. G., A. S. Sharma, K. Papadopoulos, G. Milikh, J. Lyon, and C. Goodrich (2005), Global MHD simulations of strongly driven magnetosphere: Modeling of the transpolar potential saturation, *J. Geophys. Res.*, *110*(A09203), doi:10.1029/2004JA010993.
Merkin, V. G., and J. G. Lyon (2010), Effects of the low-latitude ionospheric boundary condition on the global magnetosphere, *J. Geophys. Res.*, *115*(A), A10202.
Merkin, V. G., B. J. Anderson, J. G. Lyon, H. Korth, M. Wiltberger, and T. Motoba (2013), Global evolution of Birkeland currents on 10 min timescales: MHD simulations and observations, *J. Geophys. Res.*, *118*(8), 4977–4997.
Ogino, T., and R. J. Walker (1984), A magnetohydrodynamic simulation of the bifurcation of tail lobes during intervals with a northward interplanetary magnetic field, *Geophys. Res. Lett.*, *11*, 1018–1021, doi:10.1029/GL011i010p01018.
Ohtani, S., S. Wing, P. T. Newell, and T. Higuchi (2010), Locations of night-side precipitation boundaries relative to R2 and R1 currents, *J. Geophys. Res.*, *115*, A10233, doi:10.1029/2010JA015444.
Ohtani, S., S. Wing, V. G. Merkin, and T. Higuchi (2014), Solar cycle dependence of nightside field-aligned currents: Effects of dayside ionospheric conductivity on the solar wind-magnetosphere-ionosphere coupling, *J. Geophys. Res.*, *119*(1), 322–334, doi:10.1002/2013JA019410.
Pembroke, A., F. Toffoletto, S. Sazykin, M. Wiltberger, J. Lyon, V. Merkin, and P. Schmitt (2012), Initial results from a dynamic coupled magnetosphere-ionosphere-ring current model, *J. Geophys. Res.*, *117*, A02211.
Pulkkinen, A., et al. (2011), Geospace environment modeling 2008–2009 challenge: Ground magnetic field perturbations, *Space Weather*, *9*, S02004, doi:10.1029/2010SW000600.
Raeder, J., D. Larson, W. Li, E. L. Kepko, and T. Fuller-Rowell (2008), OpenGGCM Simulations for the THEMIS mission, *Space Sci. Rev.*, *141*, 535–555, doi:10.1007/s11214-008-9421-5.
Rastätter, L., M. M. Kuznetsova, A. Vapirev, A. Ridley, M. Wiltberger, A. Pulkkinen, M. Hesse, and H. J. Singer (2011), Geospace environment modeling 2008–2009 challenge: Geosynchronous magnetic field, *Space Weather*, *9*, S04005, doi:10.1029/2010SW000617.
Richmond, A. D. (1992), Assimilative mapping of ionospheric electrodynamics, *Adv. Space Res.*, *12*, 59–68, doi:10.1016/0273-1177(92)90040-5.
Roelof, E. C. (1989), Remote sensing of the ring current using energetic neutral atoms, *Adv. Space Res.*, *9*(12), 195–203.
Schunk, R. W., et al. (2004), Global Assimilation of Ionospheric Measurements (GAIM), *Radio Science*, *39*, RS1S02, doi:10.1029/2002RS002794.
Shprits, Y., A. Kellerman, D. Kondrashov, and D. Subbotin (2013), Application of a new data operator-splitting data assimilation technique to the 3-D VERB diffusion code and CRRES measurements, *Geophys. Res. Lett.*, *40*(19), 4998–5002, doi:10.1002/grl.50969.
Sitnov, M. I., N. A. Tsyganenko, A. Y. Ukhorskiy, B. J. Anderson, H. Korth, A. T. Y. Lui, and P. C. Brandt (2010), Empirical modeling of a CIR-driven magnetic storm, *J. Geophys. Res.*, *115*, A07231.
Toffoletto, F., S. Sazykin, R. Spiro, and R. Wolf (2003), Inner magnetospheric modeling with the Rice Convection Model, *Space Sci. Rev.*, *107*(1), 175–196.
Tóth, G., D. L. de Zeeuw, T. I. Gombosi, W. B. Manchester, A. J. Ridley, I. V. Sokolov, and I. I. Roussev (2007), Sun-to-thermosphere simulation of the 28–30 October 2003 storm with the Space Weather Modeling Framework, *Space Weather*, *5*(6), S06003, doi:10.1029/2006SW000272.
Vasyliunas, V. M. (1970), Mathematical models of magnetospheric convection and its coupling to the ionosphere, *Particles and Field in the Magnetosphere*, *17*, 60. [Available at http://link.springer.com/chapter/10.1007/978-94-010-3284-1_6.]
Waters, C. L., B. J. Anderson, and K. Liou (2001), Estimation of global field aligned currents using the Iridium® System magnetometer data, *Geophys. Res. Lett.*, *28*(1), 2165–2168.
Wing, S., S.-I. Ohtani, P. T. Newell, T. Higuchi, G. Ueno, and J. M. Weygand (2010), Dayside field-aligned current source regions, *J. Geophys. Res.*, *115*(A12), A12215, doi:10.1029/2010JA015837.
Wolf, R. A. (1983), The quasi-static (slow-flow) region of the magnetosphere, in *Solar-Terrestrial Physics*, edited by R. L. Carovillano and J. M. Forbes, pp. 303–368, D. Reidel Comp., Dordrecht/Boston/Lancaster.
Xi, S., W. Lotko, B. Zhang, O. J. Brambles, J. G. Lyon, V. G. Merkin, and M. Wiltberger (2015), Poynting flux-conserving low-altitude boundary conditions for global magnetospheric models, *J. Geophys. Res.*, *120*, 384–400, doi:10.1002/2014JA020470.